Formation of Small Silica Aggregates by Turbulent Aggregation

Frédéric Gruy

Formation of small silica aggregates by turbulent aggregation

Frédéric GRUY

Ecole des Mines de Saint-Etienne, 158 Cours Fauriel,

42023 SAINT ETIENNE Cedex 2, FRANCE

running title : formation of small silica aggregates by turbulent aggregation

correspondence : Dr F. Gruy

Ecole des Mines de Saint-Etienne, 158 Cours Fauriel,

42023 SAINT ETIENNE Cedex 2, FRANCE

ABSTRACT

Aggregation of silica powder in water has been experimentally studied by turbidimetry. Aggregation was carried out in a stirred tank under physicochemical conditions corresponding to attractive inter-particle forces. The effect of different primary particle sizes and stirring rates on aggregation dynamics has been studied. The scattering cross sections of silica aggregates were calculated in the framework of the Anomalous Diffraction (AD) approximation of light scattering theory. Aggregation has been studied by using Kusters's and Brakalov's approaches. By comparison between experimental and theoretical turbidity changes with time it has been shown that aggregates are small and slightly porous. The aggregation process is characterised by a weak fractal dimension D_{wf} and an aggregate limit size L. D_{wf} is found in the range [2.4-2.5]. D_{wf} (respectively L) is a weakly increasing (respectively decreasing) function of the stirring rate or of the shear rate.

KEY WORDS

aggregation, fractal, turbulence, breakage, optical properties, light scattering

INTRODUCTION

Aggregation occurs in many biological, chemical and physical processes. It often concerns suspension of small particles in a liquid. Dynamics of aggregation mainly depends on the hydrodynamic conditions and on the particle size. In still media, aggregation of submicronic particles is due to Brownian encounters, whereas larger particles undergo sedimentation with different settling velocities and therefore collide and may aggregate. However, in many practical situations, it is necessary to put the solid-liquid suspension in motion to homogenise it or to convey it. In this case, whatever the nature of the flow, the role of the local shear flow in collisions becomes predominant. A particularly frequent application concerns the behaviour of slurries in a stirred tank, in which the flow is turbulent. For submicronic and micronic particles, aggregation takes place in the smallest eddies, the size of which is the Kolmogorov microscale η. From dimensionless considerations, η is expressed as a function of the kinematic viscosity υ and of the energy dissipation rate per unit mass ε_m in the form :

$$\eta = \left(\frac{\upsilon^3}{\varepsilon_m} \right)^{1/4} \qquad [1]$$

The velocity gradient or shear rate $\dot{\gamma}$ in each eddy is proportional to $\left(\frac{\varepsilon_m}{\upsilon} \right)^{1/2}$.

If the suspension initially consists of one kind of particle, so-called primary particle, aggregation leads to the formation of well-defined aggregates. At a given time, there is a polydisperse aggregates population in the liquid medium.

AGGREGATION

Aggregation is the consequence of a collision between particles. The mechanism which brings particles into close proximity results from the hydrodynamics of the suspension. An

aggregate is characterised by its number *i* of primary particles (supposed to be identical). Aggregation between *i*-mer and j-mer may be represented by the quasi chemical equation :

$$i\text{-mer} + j\text{-mer} \rightarrow (i+j)\text{-mer}$$

The corresponding reaction rate can be written as :

$$\frac{dN_{i+j}}{dt} = K_{i,j} N_i N_j \qquad [2]$$

where $K_{i,j}$ is the kinetic constant or kernel. N_i is the number concentration of i-mer.

As particle (aggregate) size is smaller than the Kolmogorov microscale, both Brownian kernels and turbulent kernels should be considered.

Adachi *et al.* (1) propose to express $K_{i,j}$ as the sum of two contributions :

$$K_{i,j} = (K_{i,j})_{Br} + (K_{i,j})_{turb} \qquad [3]$$

$(K_{i,j})_{Br}$ is the Brownian kernel given by Smoluchowski (2) and possibly corrected by the collision efficiency $\alpha_{i,j,Br}$:

$$(K_{i,j})_{Br} = \frac{2kT}{3\mu}(a_i + a_j)\left(\frac{1}{a_i} + \frac{1}{a_j}\right)\alpha_{i,j,Br} \qquad [4]$$

k, T and μ are respectively the Boltzmann constant, the temperature and the fluid dynamic viscosity. a_i is the radius of i-mer.

The turbulent kernel $(K_{i,j})_{turb}$ is currently written as :

$$(K_{i,j})_{turb} = \frac{4}{3}\dot{\gamma}(a_i + a_j)^3 \alpha_{i,j,turb} \qquad [5]$$

In a stirred tank, $\dot{\gamma}$ obeys the relation :

$$\dot{\gamma} = \left(\frac{3\pi}{10}\right)^{1/2}\left(\frac{\bar{\varepsilon}_m}{\upsilon}\right)^{1/2}\delta \qquad [6]$$

This relation comes from the Saffmann-Turner approach (3) ; $\bar{\varepsilon}_m$ is the mean energy dissipation rate in the tank ; δ is a correction coefficient which is introduced to take into account different deviations from this ideal model.

Many expressions are found in the literature for the mean value of ε_m , for instance (4):

$$\bar{\varepsilon}_m = \frac{N_p \omega^3 D_S^5}{V} \qquad [7]$$

N_p is the power number, D_s the stirrer diameter, ω the rotation rate of the stirrer and V the volume of the suspension. This type of expression should be used with precautions because, except for highly turbulent media, ε_m is not uniform in a stirred vessel (5). The consequence of the turbulence heterogeneity can be taken into account via δ in relation [6] .

The collision efficiency, $\alpha_{i,j,Br}$ or $\alpha_{i,j,turb}$ depends on the different interactions between particles : London-Van der Waals attractive interactions (2,6), double layer repulsive interactions (2), hydrodynamic interactions (7-9).

FRAGMENTATION OF AGGREGATES

In the aggregation processes, a maximum aggregate size is almost always observed (10-12). The corresponding mean particle size a_L (L : primary particles number) depends on shear rate, according to :

$$\frac{a_L}{a_1} \propto \dot{\gamma}^{-c} \qquad [8]$$

Exponent c is inferior to 1. Its value varies according to the authors : 0.56 in (13), 0.7 in (14), 1 in (15), 0.4 in (16), 0.6 in (17).

This can be due to two main reasons : breakage (14,18) (characterised by a fragmentation kernel) or collision efficiency becoming zero beyond a critical size (19).

In fact, the fragmentation kernels are only suitable to describe the breakage behaviour of aggregates which have "forgotten" the conditions of their formation, i.e. after strong restructuring. When an aggregate is newly formed by the collision of two smaller aggregates and does not have enough time for restructuring, the local flow shear can disrupt it into its original two components. This behaviour is particularly expected for the large aggregates which are produced during the aggregation process. Then, Brakalov (19) considers that the collision efficiency is equal to 0 when the resulting aggregate size is superior to a limit value a_L.

DYNAMICS OF AGGREGATION-FRAGMENTATION

The variation of the number concentration N_i versus time t is given by the population balance equation in its discrete form (20) :

-for $1 < i < L$

$$\frac{dN_i}{dt} = \frac{1}{2}\sum_{j=1}^{i-1} K_{j,i-j} N_j N_{i-j} - \sum_{k=1}^{\infty} K_{i,k} N_i N_k \qquad [9]$$

for $i = 1$: $$\frac{dN_1}{dt} = -\sum_{k=1}^{\infty} K_{1,k} N_1 N_k \qquad [10]$$

AGGREGATE MORPHOLOGY

The morphology of the aggregates both depends on the physicochemical and hydrodynamic conditions of their formation as well as on their intrinsic mechanical properties. However, the aggregation dynamics also depend on the morphology of the colliding particles. Recent experiments have shown that aggregates have a fractal structure (21-26). An aggregate containing i identical primary particles of radius a_1 is characterised

by : the fractal dimension D_f , the outer radius a_i. As the structure of the aggregates is non-uniform, their volume density $\phi_a(r)$ depends on the distance r from the centre of mass of the aggregate ; the average volume density is denoted $\overline{\phi_a}$ .These different characteristics are linked by the following relations (22,27) :

$$a_i = a_1\left(\frac{i}{S}\right)^{\frac{1}{Df}} \qquad [11]$$

$$\overline{\phi_a} = S\left(\frac{a_i}{a_1}\right)^{Df-3} \qquad [12]$$

where S is a structure factor.

The fractal dimension corresponding to turbulent (local shear flow) aggregation is equal to 2.35 ± 0.15 (10,17,28).

From computer simulations, Gmachowski (27) has found a relation between S and D_f which can be represented by the correlation :

$$S \approx 0.42\ D_f - 0.22 \qquad [13]$$

Sorensen *et al.* (29,30) also studied function $S(D_f)$. Contrary to Gmachowski's results, they found that S was a decreasing function of D_f. However, for fractal dimension values corresponding to shear flow aggregation ($D_f \approx 2.3$), both models give the same S value i.e. about 0.74.

Several authors have shown that only large aggregates ($i > i_{lim}$) have a fractal-like structure. For instance, Kyriakidis *et al.* (23) achieved simulations with a given aggregation mechanism. They observed that the fractal dimension of large aggregates was equal to 1.86, whereas they proved that the small aggregates were denser than the large ones. Transition value i_{lim} was found equal to 16. Adachi *et al.* (31) also found that aggregates

made of over than 50 primary particles have a fractal structure. However, small aggregates are more porous than large ones. Careful experiments of Takayasu *et al.*(32) showed that even small aggregates ($i < 5$) have a fractal-like structure.

It is suspected that aggregates in a stirred tank are generally small and not very porous.

The aim of this paper is to describe the aggregates population in a stirred reactor as accurately as possible particularly in the small size range.

This paper is organised as follows : the first part is devoted to the methodology for determining the morphology of aggregates; in the second part, we present the experimental data available on silica aggregation in a stirred tank ; the third part develops the modelling elements ; ultimately, theoretical predictions are compared to the experimental results and a global interpretation for aggregation in stirred tank is proposed.

METHODOLOGY

Characterisation of aggregates population is a difficult task. Unfortunately, no separation methods exist in order to classify a given loose aggregates population produced in a stirred tank. Only the aggregates set and not a selected aggregate size class can be analysed.

Optical methods, based on light scattering, are particularly suitable for aggregates characterisation. Over the last ten years, we have developed several optical devices to determine in situ the particle size distribution (PSD) or the moments of particulate systems. For diluted suspensions (solid volume fraction $\phi < 10^{-4}$), an optical sensor based on spectral

turbidimetry principles can be used to determine the PSD of suspensions composed of submicronic and micronic particles (33).

Turbidity τ of a monodisperse suspension of spherical particles (radius *a*) is given by the Mie theory (34) :

$$\tau(\lambda) = N\, C_{sca}(m, 2\pi a/\lambda) \qquad [14]$$

N and C_{sca} are respectively the number concentration of particles and their light scattering cross section. λ and *m* are respectively the light wavelength and the ratio of particle refractive index to surrounding medium refractive index.

The turbidity of a polydisperse suspension includes the contribution of each size class *i* of particles ($1 \le i \le n$) :

$$\tau(\lambda) = \sum_{i=1}^{n} N_i C_{sca,i} \qquad [15]$$

The time evolution of a suspension due to aggregation will be studied by spectral turbidimetry. In order to interpret the experimental results, we will use the approach involving the following procedures :

- calculation of the optical properties (in fact $C_{sca,i}$) of the aggregates possibly involved in the process ;

- prediction of number concentration ($N_i(t)$) of these aggregates from aggregation process modelling.

- calculation of the turbidity [Eq 15] and comparison to the experimental turbidity. Of course, the use of an in situ sensor will allow us the comparison between predicted and measured data throughout the aggregation process.

Both aggregation process and aggregate-light interaction are depending on aggregates morphology.

Previous and partial knowledge of the aggregation physical processes and numerous experimental data from spectral turbidimetry should allow us to improve our understanding of aggregation and to calculate the aggregates optical properties.

We chose silica as a material because different monosized powders were available. Another reason is its m value (silica in water) which is close to 1. In this case the calculation of aggregates scattering cross sections will be made easier.

EXPERIMENTAL PART

EXPERIMENTAL SET-UP, MATERIAL AND PROCEDURE

Experimental set up

The reactor used for this study of aggregation is a stirred tank the diameter *D*' of which is equal to 150 mm (Figure 1). This reactor is equipped with four baffles of width *b*. The liquid depth *H* in the vessel is equal to diameter *D*'. The bottom part of the tank is rounded. Agitation is ensured by a propeller of diameter 60 mm pumping downwards. Temperature is kept constant at 25.00°C ± 0.01°C by a double-wall jacket. The liquid volume is always equal to 2.5 L.

The turbidity probe used in this work was described by Crawley (33). It was located at the two-thirds of the vessel radius halfway between two baffles, and mounted at *z* height above the bottom of the tank with $z/H = 0.5$. The lenses / fibers set of the probe is not optically perfect. In an ideal system, only the not - scattered light reaches the detector. In fact, a small

part of the forward scattered light may be collected as well. The corresponding cone of scattered rays is characterised by its acceptance angle Ω. The latter has been estimated by comparison between experimental and calculated turbidity spectrum for high quality monodisperse latex beads (polystyrene 11.9 μm and 2.967 μm from Sigma chemical Co). Ω was found equal to 1.5°.

Material

The aggregation experiments were performed on two monodisperse silica powders. We purchased them from Geltech Company (USA) as S0501 and S1501 Geltech silica.

TEM microphotographs (Phillips CM 200) show that S0501 and S1501 Geltech silica appear as composed of spherical particles. The main size characteristics determined from TEM microphotographs analysis are summarised in Table 1. In order to be explicit, S0501 and S1501 Geltech silica will be further mentioned as silica 0.5 μm and silica 1.5 μm.

Figure 2a,b represents the zeta potential variation against pH for various values of the ionic strength *I* (measured by microelectrophoresis : Sephy, Zetaphorometer). Ionic strength and pH are fixed at a constant value by initial addition of potassium nitrate solution and nitric acid solution. The zero value of zeta potential (PZC) is reached for pH 3.2.

Determination of the optical properties of the suspension used requires knowing the values of the refractive index of these porous silica. Refractive indices n were determined by means of matching methods. Results can be represented as Cauchy's law :

for S0501 $n = 1.43905 + 3621 / \lambda^2$

for S1501 $n = 1.43394 + 3967 / \lambda^2$

with λ (nm). Geltech silica does not absorb light in the [350-750nm] wavelength range.

Experimental procedures

Figure 3 represents turbidity of silica 0.5 μm suspension versus time for various pH values. Aggregation starts at zero time. Turbidity increases with time and reaches a plateau corresponding to a presumed steady state.

With a view to simplifying the modelling, we chose to study diluted suspension aggregation in experimental conditions for which the repulsive forces between particles are very weak. A preliminary study has allowed us to determine the optimal conditions, i.e rapid aggregation. Rapid aggregation corresponds to pH = 2.44 (and I = 0.01 M).

Each experiment consists of the following different steps :

(i) filling the reactor with 2.22 L of pure water ; dissolution of 1.61 g potassium nitrate ;

(ii) starting thermal control and stirring ;

(ii) measuring of the blank turbidity (without solid) ;

(iii) silica powder is dispersed for 15 min with ultrasonics in a small vessel containing 0.2 L of pure water. The powder weight is 0.424 g, i.e $\phi = 7.54\ 10^{-5}$. Then, this suspension is poured into the reactor ;

(iv) pH is fixed at 2.44 by addition of a few drops of nitric acid solution. Suspension destabilisation occurs.

At experiment end, a small quantity of suspension is sampled, dried at 120°C and examined by optical microscopy (Axioskop, Zeiss company).

EXPERIMENTAL RESULTS

Influence of primary particle size

Figure 4 and 5 represent turbidity-time evolution for various wavelengths and respectively for silica 0.5 μm and 1.5 μm. For the smaller primary particle size, turbidity

increases, then reaches a plateau ; for the larger primary particle size, turbidity decreases, then reaches a plateau. These different behaviours will be explained by aggregate optical properties, which depend on the primary particle size.

Suspensions corresponding to the plateau were examined by optical microscopy. Because of primary particle size, only silica 1.5 μm suspensions can be observed. Even if the sampling cannot lead to accurate measurements, one may conclude that the aggregates always contain less than thirty primary particles.

Influence of the stirring rate

Figure 6 represents turbidity time evolution for different stirring rates for 0.5 μm silica. Generally speaking, the behaviour of diluted silica suspensions is similar to the behaviour we observed for diluted titania (17) and alumina (28) suspensions. More particularly the same qualitative dependence of both initial and large time characteristics of the aggregating suspension against the stirring rate is observed here. As expected, the higher the stirring rate, the higher the initial aggregation rate (initial slope of the turbidity-time curve). Whatever the stirring rate, a plateau is reached. The final turbidity value can be easily linked to the granular state of the system. For diluted titania (17) and alumina (28) suspensions, increasing the stirring rate results in reducing the aggregate mean size at the steady state. It is not so clear for 0.5 μm silica (see below).

MODELLING

Whatever the experiments, the silica aggregates formed in the system are small (see above). Standard relations [Eq. 11,13], which express the relationship between their size and the number of monomers they consist in, have to be carefully used.

SMALL AGGREGATE MORPHOLOGY

For small aggregates ($i < i_{lim}$), an alternative approach can be attempted. It consists in building an aggregates set type (i = 1,2,4,8,16,32 ...). For instance, a set of aggregates with small porosity may consist of doublet (i=2), tetrahedron (i=4), cube (i=8), ... These aggregates are not fractal-like. The set of integers (defined by $i = 2^j$) is suitable for the chosen aggregates classes for aggregation modelling (18). Most developments in aggregation theory and optical properties modelling correspond to spherical particles. In these two fields, the relevant parameter is the projected area Sp of the sphere on a plane. Thus, we define radius $a_{i,e}$ of the equivalent sphere for an aggregate as :

$$\pi a_{i,e}^2 = < Sp >_O \qquad [16]$$

where $< Sp >_O$ is the average projected area according to all aggregate orientations. Then, the average volume density is $\bar{\phi}_a = i (a_1 / a_{i,e})^3$.

Nevertheless, it is possible to associate a fractal dimension to a well-built set by assuming that a given set element has the same average volume density as the fractal aggregate with the same primary particles number. Then, we may characterize a given aggregates set by the previously defined and weak (in the mathematical meaning of the word) fractal dimension D_{wf}. This new definition can be only applied to aggregates with high (quasi spherical) symmetry. The so-defined aggregates contain accurately located primary

particles. Hence, this description is more realistic than an enlargement of a fractal one to small aggregates.

During aggregation process, small and large aggregates are present. If $i < i_{lim}$, aggregates are assumed to belong to a given aggregates set characterised by a weak fractal dimension D_{wf} ; if $i > i_{lim}$, aggregates are considered as fractal with the same fractal dimension.

We define several aggregates families (sets), called S_1, S_2, S_3, each one characterised by its weak fractal dimension D_{wf} (Figure 7a). For sets S_2 and S_3, lines between primary particles represent allowed contacts ; however, a given particle can be located anywhere around its neighbours due to possible free rolling (Figure 7b). In this case, ratio $\frac{a_{i,e}}{a_1}$ will be an average ratio according to all possible aggregate conformations.

Table 2 contains for each aggregate the corresponding ratio $\frac{a_{i,e}}{a_1}$. Values corresponding to the classical mechanisms BCCA (Ballistic Cluster-Cluster Aggregation) and BCCA-R (BCCA with Restructuring) have been calculated by Meakin (35). The very large aggregates are fractal-like and their fractal dimensions D_f are 1.95 (BCCA) and 2.12 (BCCA-R). It can be noted that aggregates family S_3 and BCCA aggregates have the same $\frac{a_i}{a_1}$ values. BCCA-R aggregates $\frac{a_i}{a_1}$ values are between ones of S_1 set and S_2 set. However, when i increases, S_2 and BCCA-R aggregates are more and more similar with respect to the $\frac{a_i}{a_1}$ values. For $D_f > 2$ and in the limit $i \to \infty$ Meakin showed that $\frac{a_i}{a_1} \propto \frac{a_{i,e}}{a_1} \propto i^{\frac{1}{Df}}$. Then, we can consider that with the limit $i \to 1$, $\frac{a_{i,e}}{a_1} \propto i^{\frac{1}{Dwf}}$.

SMALL AGGREGATE OPTICAL PROPERTIES

Fundamentals

Each aggregate is characterised by its diameter and its mean inner volume fraction $\bar{\phi}_a$. To our knowledge, accurate calculation of aggregate scattering cross-sections is not yet completed for any primary particle size. Nevertheless, calculations were achieved when primary particle is a Rayleigh or Rayleigh-Debye-Gans (RDG) scatterer. Two kinds of modelling are used to calculate optical properties of porous materials :

i. effective refractive index method

The easiest way to determine the optical properties of an aggregate is to calculate its effective refractive index m_a (see for instance ref 36). The equation derived by Maxwell-Garnett has been proved to be suitable :

$$\frac{(m_a^2 - 1)}{(m_a^2 + 2)} = \bar{\phi}_a \frac{(m^2 - 1)}{(m^2 + 2)} \qquad [17]$$

m and m_a are the relative refractive indices respectively for primary particles and aggregates.

Given the diameter and the effective refractive index of an aggregate, the Mie theory (34) allows us to calculate the scattering cross section C_{sca} for a given wavelength.

ii. interferences method

Generally, the object (primary particle, aggregate ...) can be divided into smaller identical parts (elements). Each element is polarisable. In the presence of a variable electric field, the element becomes an oscillating dipole, which itself creates an electromagnetic

field. When an object is illuminated by an electromagnetic wave, each element receives the incident electric field and the one coming from the other elements. As a result, one may associate an oscillating dipole moment to each element. Thus, the object emits an electromagnetic wave (scattered wave), which includes the contribution of each oscillating dipole.

Most often, the incident wave is randomly polarised and the object (scatterer) can randomly orientate. Thus, the optical properties are obtained after calculating an average over all the wave polarisation states and object orientations.

Table 3 presents several models, each one characterised by the polarisable element, the object, the calculation type.

If the object is an aggregate, the element may be either the whole primary particle or a part of the primary particle.

The Khlebtsov procedure, similar to Percival-Berry one, has been applied to aggregates of many particles (fractal aggregates). Rayleigh-Debye-Gans scatterers are characterized by $m-1\langle\langle 1$ and $\frac{4\pi}{\lambda}a_1(m-1)\langle\langle 1$. However, when $\frac{4\pi}{\lambda}a_1(m-1)$ is not so small, anomalous diffraction occurs (34). In the Rayleigh-Debye-Gans domain, there is interference of light waves which are independently scattered by all small volume elements. In the anomalous diffraction domain, there is straight transmission and subsequent diffraction. In this case, the scattered intensity is concentrated near the original direction of propagation and the extinction cross section obeys the relation (34) :

$$C_{ext} = 2\iint_{[Sp]}(1-\cos\frac{2\pi}{\lambda}\delta(m-1))dS_p \qquad [18]$$

Integration is performed over the object projected area S_p on a plane perpendicular to propagation direction. δ is the path travelled through the object. This calculated path is a function of the projection coordinates.

Optical properties of primary particle

One of the relevant parameters for material optical properties is m-1. In the case of Geltech amorphous silica, m-1 is equal to about 0.08. Size parameter α (= $2\pi a_1/\lambda$) is equal to 3.66 (0.5 μm silica) and 10.1 (1.5 μm silica) for λ = 600nm. As (m-1)α is inferior to 1 the two primary particles behave as RDG scatterers (Table 4).

As expected, as we increase the size of the particle, its behaviour differs more and more from the RDG scatterer.

Optical properties of small aggregate

** 0.5 μm silica*

Tables 5a (λ = 752.8 nm) and 5b (λ = 401.9nm) compare aggregates (set S_1) scattering cross sections calculated from different models :

- effective refractive index (ERI) method
- Percival-Berry-Khlebtsov (PBK) method applied to small aggregates
-anomalous diffraction (AD) approximation
-compact sphere (CS) with the same material quantity

Results are shown as the ratio of actual scattering cross section to the sum of aggregate primary particles cross sections $C_{sca,i} / (iC_{sca,1})$.

Table 5c compares aggregates scattering cross sections calculated from AD method for the three aggregates sets S_1, S_2 and S_3.

We can conclude that :

- contrary to CS model, the three methods (ERI, PBK, AD) give almost the same values with a ten per cent correspondence rate for λ = 752.8 nm. For λ = 401.9 nm, only ERI and AD methods result in the same scattering cross sections. It is not surprising in so far as silica particles are no more RDG scatterers for small wavelength (λ = 401.9 nm).

- the denser the aggregates, the higher the scattering cross sections.

** 1.5 μm silica*

Table 6a (λ = 752.8 nm) compares aggregates (S_1) scattering cross sections calculated from different models (CS, ERI, PBK, AD). Results are shown as the ratio of actual scattering cross section to the sum of aggregate primary particles cross sections.

As expected, PBK and AD methods result in different values of any scattering cross section. PBK is only valid for RDG scatterers ; aggregates of 1.5 μm silica undergo anomalous diffraction. ERI method gives scattering cross section values close to AD ones. It will be noted that the difference between ERI and AD values increases as the primary particles number increases or/and, as the light wavelength decreases (not shown in tables). ERI method is rigorously equivalent ($m \rightarrow 1$) to AD method applied to porous spheres with radius $a_{i,e}$ and porosity 1-$\bar{\phi}_a$. The light path travelled through the porous sphere is $\bar{\phi}_a$ times the path travelled through the compact sphere with the same radius.

Although ERI method is not rigorous, it is sufficient for simple calculation, particularly as detector acceptance angle is not equal to zero.

Table 6b compares aggregates scattering cross sections calculated from AD method for the three aggregates sets S_1, S_2 and S_3.

As for 0.5 μm silica, the denser the aggregates, the higher the scattering cross sections.

As previously indicated, the detector acceptance angle has to be taken into account for effective scattering cross section calculations. This is easily done for ERI, PBK methods. Unfortunately, it is more difficult for anomalous diffraction (34). Considering the similarity between ERI and AD methods ($\Omega = 0$), we will apply the following relation for the actual corrected scattering cross section :

$$C_{sca}^{AD}(\Omega) = C_{sca}^{AD}(0)\frac{C_{sca}^{ERI}(\Omega)}{C_{sca}^{ERI}(0)} \qquad [19]$$

AGGREGATION DYNAMICS

Aggregation is treated as previously recalled (cf § introduction). Aggregates are considered as belonging to S_1,S_2 or S_3 sets. Their radii will be given by equation 16.

Under the present operating conditions (pH, ionic strength), only attractive forces between particles should be considered. Hamaker's constant A is equal to 1 x 10^{-20} J for silica in water (42). The two collision efficiencies will be calculated following :

Brownian collision efficiency

For particle size over 0.5 μm, the contribution of Brownian kernel to $K_{i,j}$ is minor. An approximative value for $\alpha_{i,j,Br}$ is sufficient. It was taken equal to 0.5 in the experimental work of Adachi *et al.* (1) and Kyriakidis *et al.* (23).

Turbulent collision efficiency

spherical particles

Calculation of collision efficiency should take into account the contribution of the three types of the above-mentioned interactions (7-9,11,43-45).

non-compact aggregates

In this work, we follow the procedure proposed by Kusters *et al.* (10,22) (*shell-core* approach) to calculate the collision efficiency $\alpha_{i,j,turb}$ between two porous aggregates. $\alpha_{i,j,turb}$ is expressed as a function of the permeability κ_i of the bigger particle, itself depending on the particle morphology.

The numerical constants δ (equation [6]) and Np (equation [7]) have been taken equal to 0.7 (10) and 0.36, a value commonly assumed for a marine-type mixing propeller (46).

Aggregates limit size is obtained by using the zero collision efficiency approach.

The time evolution of the particle size distribution is simulated by solving the population balance equations [9, 10]. The involved procedure consists in considering aggregates classes. Class j is centered around the aggregate composed of 2^j primary particles (18).

COMPARISON OF EXPERIMENTS AND MODELLING - DISCUSSION

Aggregation dynamics at a very short time level

At the beginning of aggregation, the suspension only contains primary particles and doublets. The early stage of aggregation occurs without fragmentation. The aggregation rate can be written as :

$$\frac{dN_1}{dt} = -K_{1,1} N_1^2$$

with $N_1 + 2N_2 = N_1(t=0)$

The suspension turbidity obeys the relation :

$$\tau = C_{sca,1} N_1 + C_{sca,2} N_2$$

then $(\frac{d\tau}{dt})_{t=0} \approx -(C_{sca,1} - \frac{1}{2} C_{sca,2}) K_{1,1} N_1^2 (t=0)$

Experiments have been carried out with 0.5 μm silica for various stirring rates and solid volume fractions (at λ = 652 nm). Whatever the solid volume fraction, K_{11} (m^3/s) can be expressed as a function of stirring rate ω (rps) :

$$K_{1,1} = 2.5 10^{-18} + 2.2 10^{-18} \omega^{0.9} \qquad [20]$$

The first term (on the rhs) is the Brownian contribution for K_{11}. The second one is the contribution of turbulent aggregation.

For two equally sized micronic spheres, Van de Ven (8) showed that :

$$\alpha_{1,1,turb} = \left(\frac{A}{36\pi \mu \dot{\gamma} a^3} \right)^n$$

From calculation (8,45), n was found equal to 0.18.

Then, $(K_{1,1})_{turb} = \frac{4}{3}\dot{\gamma}(2a_1)^3\left(\frac{A}{36\pi\mu\dot{\gamma}a^3}\right)^n \propto \dot{\gamma}^{1-n} \propto \omega^{3(1-n)/2}$ [21]

Hence exponent n derived from our experiments is equal to 0.4. This value, which is higher than Van de Ven's, is closer to other experimental values (13, 47). However, experimental results [Eq 20] and calculation [Eq 6,7,21] are in agreement with a ten per cent correspondence rate.

The theoretical Brownian kernel $(K_{1,1})_{Br}$ is equal to 6.1 10^{-18} m^3/s. We supposed that the difference between experimental and theoretical values is due to a collision efficiency of 0.2 instead of 0.5.

It will be pointed out that analysis of turbidity evolution is very sensitive to the values of particles scattering cross section. As $\frac{(\frac{1}{2}C_{sca,2} - C_{sca,1})}{C_{sca,1}} << 1$ for silica in water, a small error in scattering cross section estimate leads to an erroneous kinetic constant value. This remark is still valid considering the whole aggregation process.

Aggregation dynamics at longer time level

In order to simulate the turbidity change with time, we can try :

- different methods for scattering cross section calculation : ERI, PBK, AD
- different aggregates sets : S_1, S_2 or S_3
- various aggregate limit sizes L.

Methods for scattering cross section calculations lead to different turbidity changes with time only for 1.5 μm silica aggregation. Figure 8 shows the influence of scattering cross section

modelling (PBK,AD) on turbidity – time curve (1.5 μm silica ; λ = 501.7 nm ; S_2 ; L = 16). As expected, PBK calculations do not correctly describe the optical properties of 1.5 μm silica aggregates. Contrary to experiment, simulated turbidity (PBK) increases with time. From now on, AD method will be chosen for both silica primary particles.

Figures 9a and 9b compare, for 0.5 μm and 1.5 μm silica, the influence of aggregates sets (S_1,S_2,S_3) on turbidity – time curves (λ = 501.7 nm). Figures 10a and 10b compare for 0.5 μm and 1.5 μm silica the influence of aggregate limit size (L = 8, 16, 32) on turbidity – time curves (S_2 ; λ = 501.7 nm). Figures 10a and 10b show that the higher L, the bigger the difference between initial and final turbidity. The initial aggregation rate is a little sensitive to set choice (Figures 9a, 9b). Behaviours of S_2 and S_3 are similar. The different final turbidity values are due to the difference in scattering cross sections. The denser the aggregate, the higher the scattering cross section and the turbidity.

Figures 11a and 11b show the turbidity change with time (ω = 450 rpm) for 0.5 μm and 1.5 μm silica and various wavelengths. The closest to superimposition is obtained as the aggregate set is S_2 and the larger aggregate contains 32 (0.5 μm silica) or 16 (1.5 μm silica) primary particles. L values are in accordance with our suspension observations by optical microscopy and results of other researchers (47). It can be seen that the simulated aggregation rate at intermediate time is a little higher than the experimental one. This is particularly true for large primary particles and short wavelengths.

Figure 12 shows for 0.5 μm silica the influence of the stirring rate on experimental and simulated turbidity evolution (λ = 501.7 nm). Table 7 represents the best modelling parameters to superimpose simulated curves on experimental ones. To analyse these curves one has to consider the initial offset of turbidity (calculation : 0.58 cm^{-1} ; experiment : 0.61 cm^{-1}). We can distinguish two behaviours, each one corresponding to a different stirring rate

range : at low stirring rates, aggregates are porous (D_{wf} = 2.4) and the limit size is high (L = 64) ; at high stirring rates, aggregates are denser (D_{wf} = 2.5) and the limit size is inferior to those determined for low stirring rates. Within each stirring rate range, refining these results is not possible. As expected, L is a decreasing function of ω and $\dot{\gamma}$. Exponent c (Eq 8) is likely to be within the range [0-0.5].

Aggregate fractal dimensions are found in the expected values range. Under high shear flow (ω = 450 rpm, 800 rpm), aggregates are more compact than those being made in a stiller medium. As shown in Table 2, the porosity difference between aggregates coming from different sets (S_1, S_2, S_3) increases with primary particles number i. Then, differences between aggregate compactness are more manifest at much higher time levels. Usually, researchers (10,17,28) assume that aggregate fractal dimension is constant with the whole stirring rate range. In the case of spherical silica primary particles, the fractal dimension of corresponding aggregates is a weakly increasing function of the stirring rate. Spicer (48) observed the same phenomenon with shear aggregation of polystyrene beads.

CONCLUSION

The aggregation of silica powder in water has been experimentally studied by turbidimetry. The aggregation was carried out in a stirred tank under physicochemical conditions corresponding to attractive inter-particle forces. The effect of different primary particle sizes and stirring rates on aggregation dynamics has been studied.

Modelling of material optical properties and aggregation was necessary to compare the experimental and theoretical turbidity changes with time. The silica / water system is characterised by a small optical contrast m-1 and a small Hamaker constant A.

Optical properties of silica aggregates in water were determined by different methods that can be applied to such a system. Anomalous Diffraction (AD) approximation of light scattering theory appears to be compatible with experimental results and the selected kind of material.

Aggregation has been studied by using :

-Kusters's approach for collision efficiency calculation

- Brakalov's approach for aggregation-fragmentation dynamics at high time levels.

We showed that :

- aggregates are small in a stirred tank

- small aggregates are slightly porous. We defined several aggregates sets and their equivalent or weak fractal dimension D_{wf}, which is found in the range [2.4-2.5]. This is also verified for the beginning of Brownian aggregation.

- aggregation process is characterised by D_{wf} and aggregate limit size L.

- D_{wf} (respectively L) is a weakly increasing (respectively decreasing) function of the stirring rate or of the shear rate.

REFERENCES

1. Adachi, Y., Cohen Stuart, M. A., and Fokkink, R., *J. Coll. Interface Sci.*, **165**, 310 (1994).
2. Verwey, E. J. W.and Overbeek, J. T. G., " Theory of the Stability of Lyophobics Colloids ", Elsevier, Amsterdam (1948).
3. Saffman, P. G., and Turner, J. S., *J. Fluid Mech.*, **1**, 16 (1956).
4. Baldi, G., Conti, R., and Alaria, E., *Chem. Eng. Sci.*, **33**, 21 (1978).
5. Kresta, S., *Can. J. Chem. Eng*,. **76**, 563 (1998).
6. Schenkel, J. H. and Kitchener, J. A., *Trans. Farad. Soc.*, **56**, 161 (1960).
7. Spielman, L. A., *J. Coll. Interface. Sci.*, **33**, 562 (1970).
8. Van de Ven, T. G. and Mason, S. G., *Colloid and Polymer. Sci.*, **255**, 468 (1977).
9. Zeichner, G. R., and Schowalter , W. R., *AIChE J.*, **23**, 243 (1977).
10. Kusters, K. A., "The influence of turbulence on aggregation of small particles in agitated vessel ", Ph.D. Thesis, Eindhoven University of Technology, The Netherlands (1991).
11. De Boer, G. B. J., Hoedemakers, G. F. M. and Thoenes, D., *Chem. Eng. Sci.*, **67**, 301 (1989).
12. Oles, V., *J. Coll. Interface Sci.*, **154**, 351 (1992).
13. Chimmili, S., Doraiswamy, D., and Gupta, R.K., *Ind. Eng. Chem. Res*. **37**, 2073 (1998).
14. Serra, T. and Casamitjana, X., *AIChE J*., **44**, 1724 (1998).
15. Serra, T., Colomer, J., and Casamitjana, X., *J. Coll. Interface Sci*, **187**, 466 (1997).

16. Higashitani, K. and Iimura, K., *J. Coll. Interface Sci*, **204**, 320 (1998).

17. Tontrup T., " Granulométrie de particules fines en suspension chargée par mesures de rétrodiffusion de lumière " Ph.D. Thesis, Ecole des Mines de Saint-Etienne, France (1999).

18. Spicer, P. T., and Pratsinis, S. E., *AIChE J.*, **42**, 1612 (1996).

19. Brakalov, L.B., *Chem. Eng. Sci*., **42**, 2373 (1987).

20. Randolph, A. D., and Larson, M. A., " Theory of Particulate Processes ", Academic Press, NewYork (1988).

21. Ayazi Shamlou, P., Stavrinides, S., Titchener-Hooker, N. and Hoare, M., *Chem. Eng. Sci.*, **49**, 2647 (1994).

22. Kusters, K. A., Wijers, J. G., and Thoenes, D., *Chem. Eng. Sci.*, **52**, 107 (1997).

23. Kyriakidis,A.S., Yiantsios, S.G., and Karabelas, A.J., *J. Coll. Interface. Sci*, **195**, 299 (1997).

24. Burns, J.L., Yan, Y, Jameson, G.J., and Biggs, S., *Langmuir*, **13**, 6413 (1997).

25. Axford, S.D.T., *J. Chem Soc Far. Trans.*, **93**, 303 (1997).

26. Thill, A., Veerapaneni, S., Simon, B., Wiesner, M., Bottero, J.Y., and Snidaro, D., *J. Coll. Interface Sci*., **204**, 357 (1998).

27. Gmachowski, L., *J. Coll. Interface Sci*., **178**, 80 (1995).

28. Saint-Raymond, H., Gruy F., and Cournil M., *J. Coll. Interface Sci*., **202**, 238 (1998).

29. Sorensen, C.M., and Roberts, G.C., *J. Coll. Interface Sci*, **186**, 447 (1997).

30. Oh, C., and Sorensen, C.M., *J. Coll. Interface Sci*, **193**, 17 (1997).

31. Adachi, Y., Kobayachi, M., and .Ooi, S., *J. Coll. Interface Sci*, **208**, 353, (1998).

32. Takayasu, M.M., and Galembeck, F., *J. Coll. Interface Sci*, **202**, 84 (1998).

33. Crawley, G. M., Cournil, M., and Di Benedetto, D., *Powder Technology*, **91**, 197 (1997).

34. Van de Hulst, H. C., " Light scattering by small particles", John Wiley, NewYork (1957).

35. Meakin, P., Donn B., Mulholland G. W., Langmuir 5(1989)510

36. Di Stasio S., Massoli P., Partec 98, 7th European Symposium Particle Characterization **I**, 169 (1998).

37. Berry, M.V., Percival, I. C., Optica Acta 33(1986)577

38. Draine, B. T., Flatau, P. J., J. Opt. Soc. Am. 11(1994)1491

39. Mulholland, G. W., Bohren, C. F., Fuller, K. A., Langmuir 10(1994)2533

40. Khlebtsov, N. G., Applied Optics 35(1996)4261

41. Xu, Y. L., Applied Optics 34(1995)4573 ; J of Computational Physics 127(1996)285

42. G.H. Bogush, C.F. Zukovski, J. Coll. Interf. Sci. 142,1(1991)19

43. Higashitani, K., Yamauchi, K., Hosokawa, G., and Matsuno, Y., J. Chem. Eng. Japan, **15**, 299 (1982).

44. Higashitani, K., Yamauchi, K., Hosokawa, G., and Matsuno, Y., J. Chem. Eng. Japan, **16**, 299 (1983).

45. Brunk, B.K., Koch, D.L., and Lion, L.W., *J. Fluid Mech*., **364**, 81 (1998).

46. Wilke, H.P., "Ruhrtechnik", Huthig Buch Verlag, Heidelberg (1991).

47. Chin, C. J., Yiacoumi, S., Tsouris, C., *J. Coll. Interface Sci*, **206**, 532 (1998).

48. Spicer, P. T., Pratsinis, S. E., Raper, J., Amal, R., Bushell, G., Meesters, G., *Powder Technology*, **97**, 26 (1998).

Material	Average number diameter (μm)	Standard deviation (μm)
S0501	0.522	0.013
S1501	1.446	0.029

Table 1 : Geltech Silica PSD Characteristics

i \ set	S_1	S_2	S_3	BCCA-R	BCCA
2	1.364	1.364	1.364	1.364	1.364
4	1.760	1.846	1.86	1.784	1.831
8	2.364	2.473	2.564	2.375	2.505
16	2.990	3.280	3.510	3.170	3.432
32	3.865	4.366	4.714	4.240	4.709
D_{wf}	2.7	2.5	2.4		

BCCA : Ballistic Cluster-Cluster Aggregation BCCA-R : BCCA with Restructuring

Table 2 : Ratio $\frac{a_{i,e}}{a_1}$ for different aggregates

Authors	element	object	calculation type	Ref
Percival-Berry	Rayleigh scatterer	any	A+MFA	37
Draine-Flatau	Electric dipole	sphere,doublet	S	38
Mulholland & Cow	Electric/magnetic dipole	Aggregate	A+S	39
Khlebtsov	RDG scatterer	Aggregate fractal-like or not	A+MFA	40
Xu	Mie scatterer	Aggregate	A+S	41

Table 3 : Different models of aggregate optical properties

A : analytical S : simulation MFA : mean field approximation

Material	S0501	S1501
$2a_1$ (μm)	0.522	1.446
exact calculation (MIE)	0.0874	4.033
RDG approximation	0.0792	4.73

Table 4 : Scattering cross sections (μm^2)

Method \ i	2	4	8	16	32
CS	1.335	1.755	2.250	2.806	3.431
ERI	1.147	1.423	1.592	2.026	2.413
PBK	1.165	1.490	1.740	2.220	2.691
AD	1.236	1.520	1.724	2.143	2.413

Table 5a : Aggregates normalised scattering cross sections

aggregates set : S_1 ; primary particles : 0.5 μm silica

λ = 752.8 nm ; C_{sca}(i = 1) = 0.0245 μm^2 ; Ω = 0°

Method \ i	2	4	8	16	32
CS		1.560	1.866	2.137	2.283
ERI		1.292	1.418	1.706	1.937
PBK		1.400	1.630	2.024	2.417
AD		1.259	1.390	1.620	1.770

Table 5b : Aggregates normalised scattering cross sections

aggregates set : S_1 ; primary particles : 0.5 μm silica

λ = 401.9 nm ; C_{sca}(i = 1) = 0.0868 μm^2 ; Ω = 0°

Method \ i	2	4	8	16	32
CS	1.335	1.755	2.250	2.806	3.431
S_1	1.236	1.520	1.724	2.143	2.413
S_2	1.236	1.398	1.602	1.832	2.085
S_3	1.236	1.383	1.537	1.668	1.735

Table 5c : Aggregates normalised scattering cross sections

primary particles : 0.5 μm silica

λ = 752.8 nm ; $C_{sca}(i = 1)$ = 0.0245 μm^2 ; $\Omega = 0°$

Method \ i	2	4	8	16	32
CS	1.208	1.402	1.527	1.510	1.265
ERI	1.054	1.220	1.307	1.468	1.533
PBK	1.137	1.409	1.636	2.037	2.425
AD	0.990	1.118	1.193	1.269	1.236

Table 6a : Aggregates normalised scattering cross sections

aggregates set : S_1 ; primary particles : 1.5 μm silica

λ = 752.8 nm ; C_{sca}(i = 1) = 1.482 μm^2 ; Ω = 0°

Method \ i	2	4	8	16	32
CS	1.208	1.401	1.527	1.508	1.266
S_1	0.990	1.118	1.193	1.269	1.236
S_2	0.990	1.049	1.112	1.170	1.175
S_3	0.990	1.048	1.089	1.100	1.100

Table 6b : Aggregates normalised scattering cross sections

primary particles : 1.5 μm silica

λ = 752.8 nm ; C_{sca}(i = 1) = 1.482 μm^2 ; Ω = 0°

ω	Aggregates set	L
0	S3	> 64
150	S3	64
450	S2	32
800	S2	32

Table 7 : Parameters for calculated turbidity-time function (Figure 12)

LEGENDS OF FIGURES

Figure 1 : Schematic representation of the aggregation reactor ($H = D'$; $D_S = 0.33\ D'$; $b = 0.1\ D'$; $c = 0.33\ D'$; $f = 0.02\ D'$)

Figure 2a,b : Silica zeta potential as a function of pH at various ionic strength values *I*.

a : 0.5 μm silica **b : 1.5 μm silica**

Figure 3 : Turbidity change with time due to the aggregation process for various pH (experimental conditions : **0.5 μm silica** *;* T = 25 °C ; ω = 450 rpm ; $\phi = 7.54 \times 10^{-5}$; I = 0.01 mol. L^{-1} ; λ = 501.7 nm)

Figure 4 : Turbidity change with time for various light wavelengths (experimental conditions : **0.5 μm silica** ; T = 25 °C ; pH = 2.44 ; ω = 450 rpm ; $\phi = 7.54 \times 10^{-5}$; I = 0.01 mol. L^{-1})

Figure 5 : Turbidity change with time for various light wavelengths (experimental conditions : **1.5 μm silica** ; T = 25 °C ; pH = 2.44 ; ω = 450 rpm ; $\phi = 7.54 \times 10^{-5}$; I = 0.01 mol. L^{-1})

Figure 6 : Influence of stirring rate on turbidity time evolution during **0.5 μm silica** aggregation (experimental conditions : pH = 2.44 ; T = 25 °C ; $\phi = 7.54 \times 10^{-5}$; I = 0.01 mol. L^{-1} ; λ = 501.7 nm) **;**

Figure 7a : Aggregates sets : S_1, S_2 and S_3

Figure 7b : Possible aggregate conformations (S_3 ; i = 4)

Figure 8 : Influence of optical properties modelling (PBK,AD) on calculated turbidity time evolution (**1.5 μm silica** ; T = 25 °C ; pH = 2.44 ; ω = 450 rpm ; ϕ = 7.54 x 10^{-5} ; I = 0.01 mol. L^{-1} ; λ = 501.7 nm)

Figure 9 : Influence of aggregates morphology modelling (S_1, S_2 and S_3 ; L = 16) on calculated turbidity time evolution (T = 25 °C ; pH = 2.44 ; ω = 450 rpm ; ϕ = 7.54 x 10^{-5} ; I = 0.01 mol. L^{-1} ; λ = 501.7 nm) **a : 0.5 μm silica** **b : 1.5 μm silica**

Figure 10 : Influence of aggregate limit size (S_2 ; L = 8,16,32) on calculated turbidity time evolution (T = 25 °C ; pH = 2.44 ; ω = 450 rpm ; ϕ = 7.54 x 10^{-5} ; I = 0.01 mol. L^{-1} ; λ = 501.7 nm) **a : 0.5 μm silica** **b : 1.5 μm silica**

Figure 11 : Comparison between experimental and calculated turbidity time evolution for various light wavelengths (experimental conditions : T = 25 °C ; pH = 2.44 ; ω = 450 rpm ; ϕ = 7.54 x 10^{-5} ; I = 0.01 mol. L^{-1})

a : 0.5 μm silica (S_2 ; L = 32) **b : 1.5 μm silica** (S_2 ; L = 16)

Figure 12 : Comparison between experimental and calculated turbidity time evolution for various stirring rates (experimental conditions : **0.5 μm silica** ; pH = 2.44 ; T = 25 °C ; ϕ = 7.54 x 10^{-5} ; I = 0.01 mol. L^{-1} ; λ = 501.7 nm)

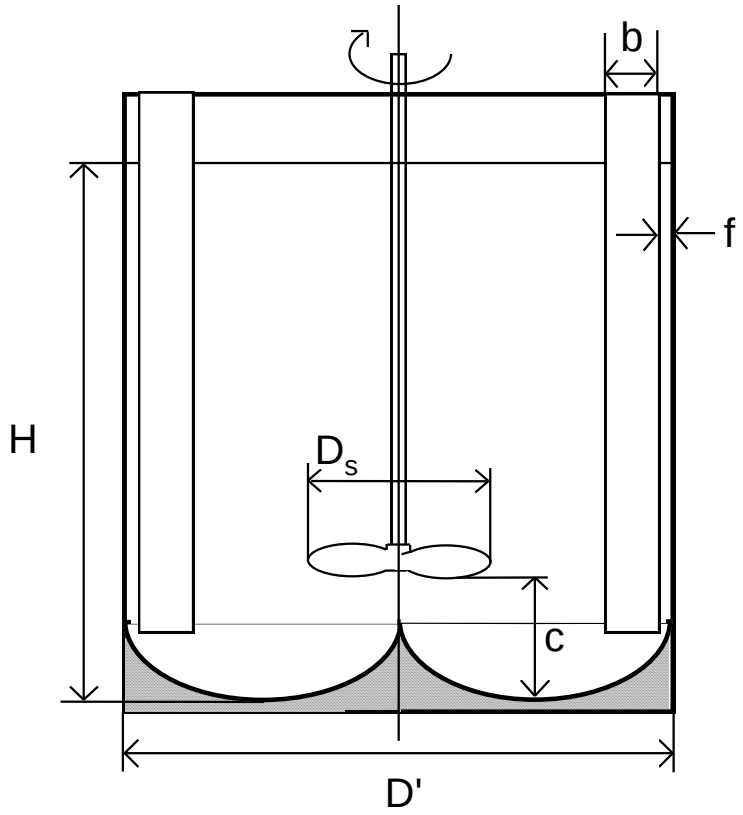
b
f
H
D_s
c
D'

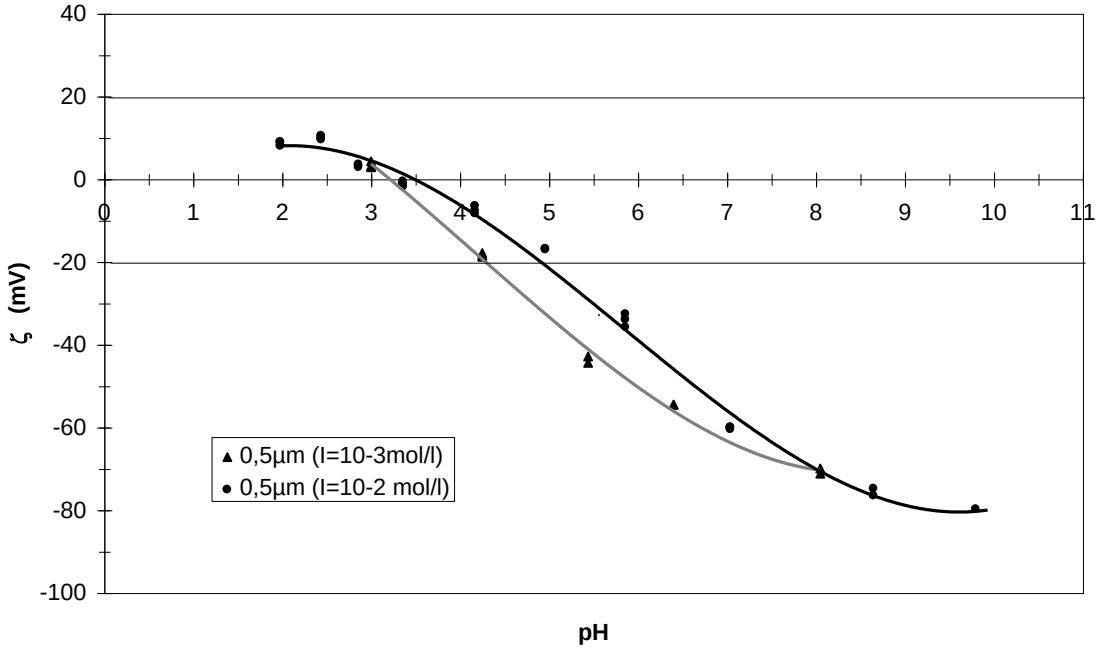
40
20
0
-20
-40
-60
-80
-100
0
1
2
3
4
5
6
7
8
9
10
11
ζ (mV)
pH
▲ 0,5µm (I=10-3mol/l)
● 0,5µm (I=10-2 mol/l)

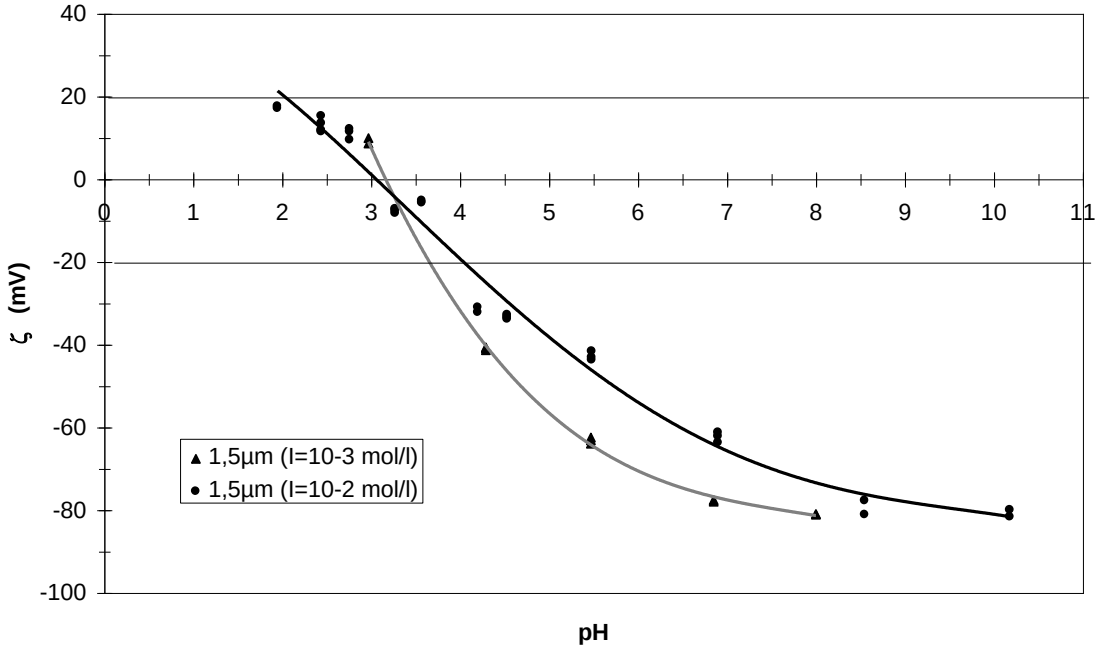
40
20
0
-20
-40
-60
-80
-100
0
1
2
3
4
5
6
7
8
9
10
11
ζ (mV)
pH
▲ 1,5µm (I=10-3 mol/l)
● 1,5µm (I=10-2 mol/l)

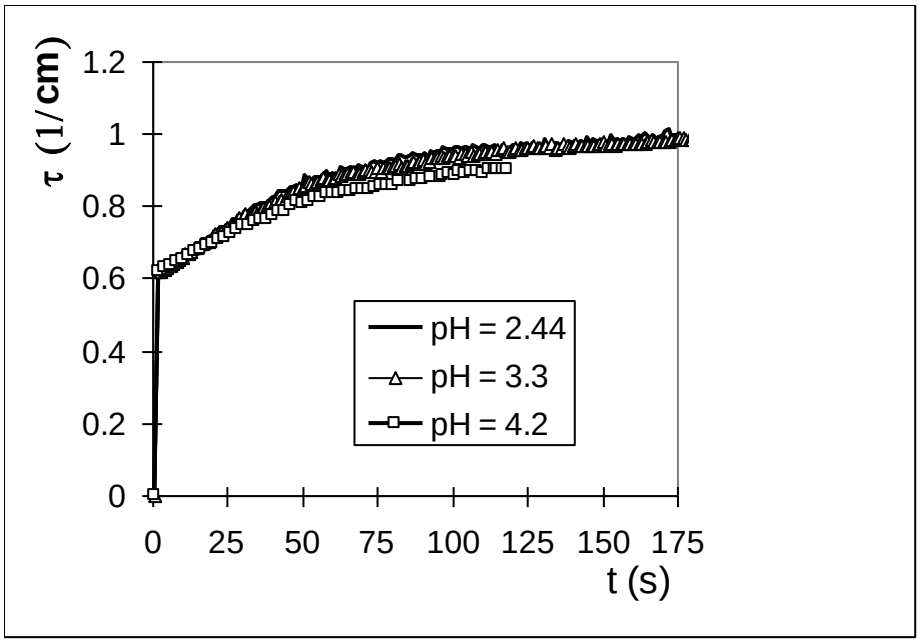
τ (1/cm)
1.2
1
0.8
0.6
0.4
0.2
0
0
25
50
75
100
125
150
175
t (s)
pH = 2.44
pH = 3.3
pH = 4.2

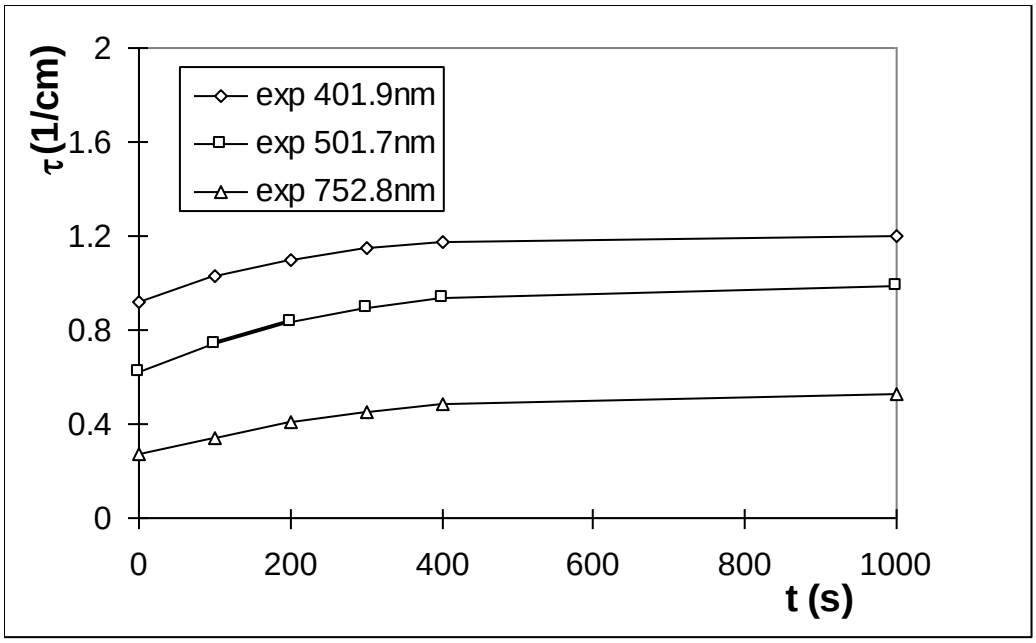
τ(1/cm)
2
1.6
1.2
0.8
0.4
0
0
200
400
600
800
1000
t (s)
exp 401.9nm
exp 501.7nm
exp 752.8nm

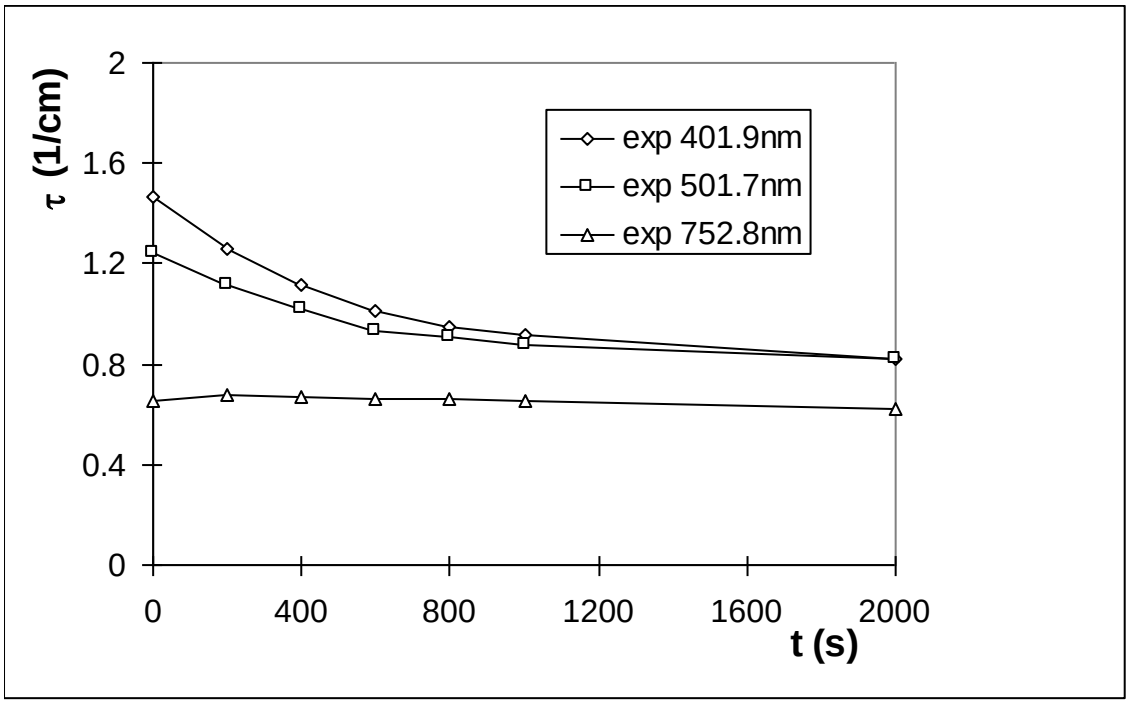
τ (1/cm)
2
1.6
1.2
0.8
0.4
0
0
400
800
1200
1600
2000
t (s)
exp 401.9nm
exp 501.7nm
exp 752.8nm

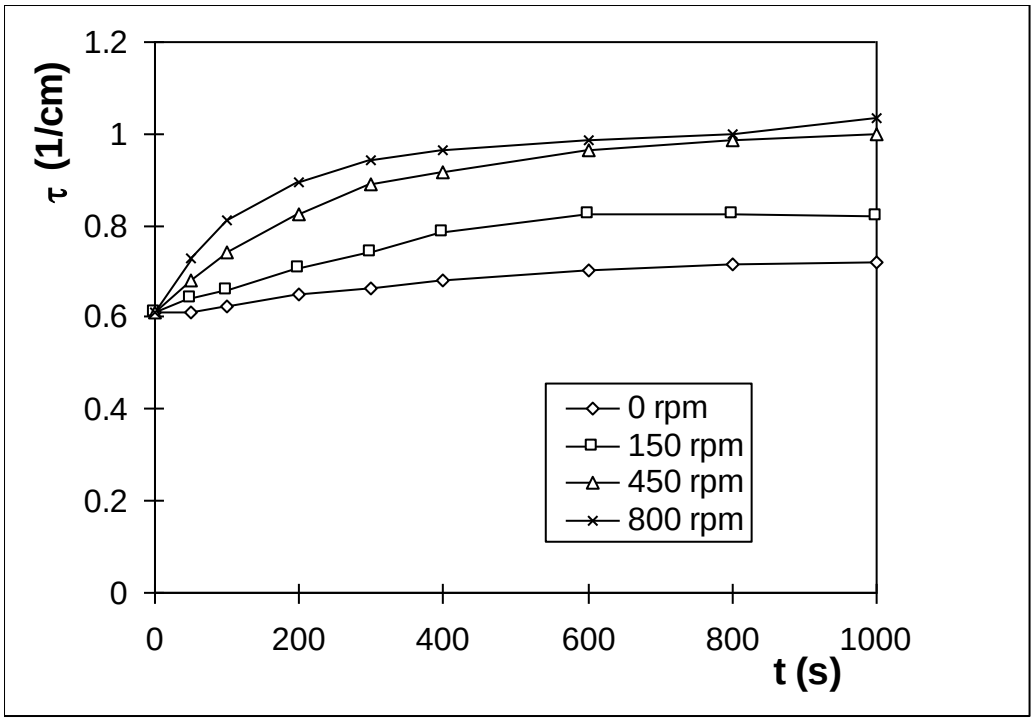
τ (1/cm)
1.2
1
0.8
0.6
0.4
0.2
0
0
200
400
600
800
1000
t (s)
0 rpm
150 rpm
450 rpm
800 rpm

i		S_1	S_2	S_3
1				
2	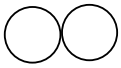			
4				
8		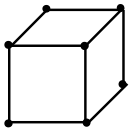	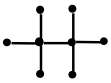	
16		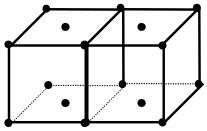	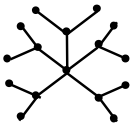	
32		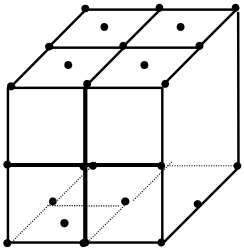	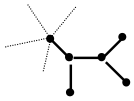	

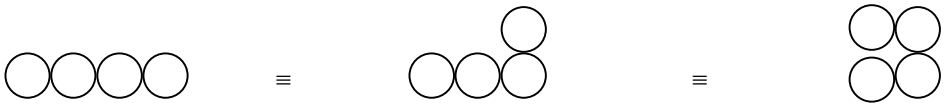

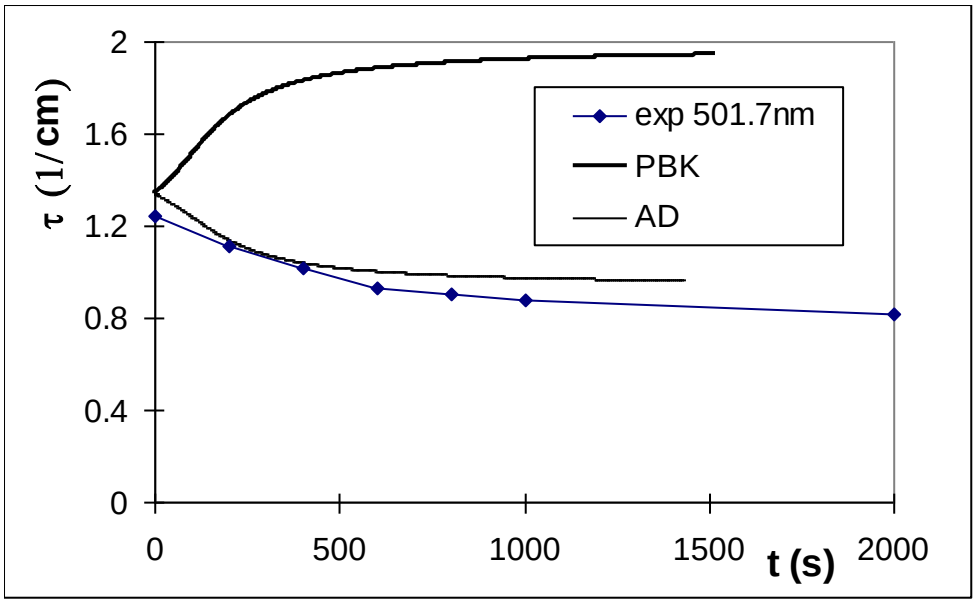
2
1.6
1.2
0.8
0.4
0
τ (1/cm)
0
500
1000
1500
2000
t (s)
exp 501.7nm
PBK
AD

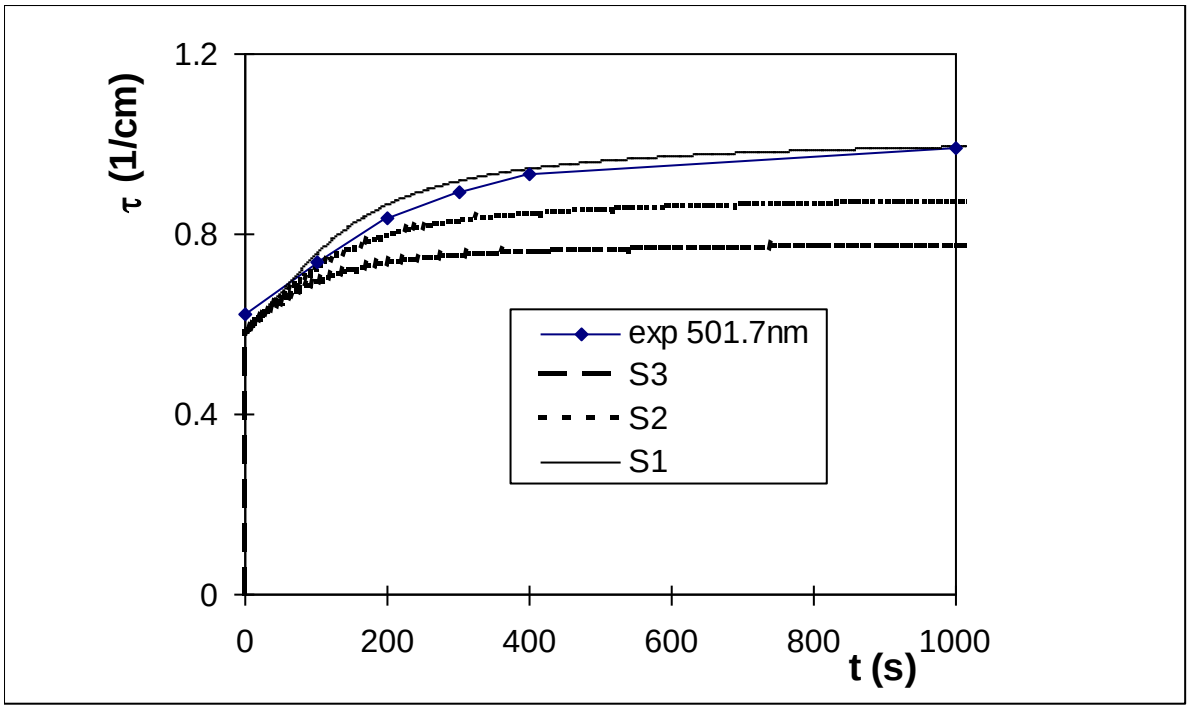
τ (1/cm)
1.2
0.8
0.4
0
0
200
400
600
800
1000
t (s)
exp 501.7nm
S3
S2
S1

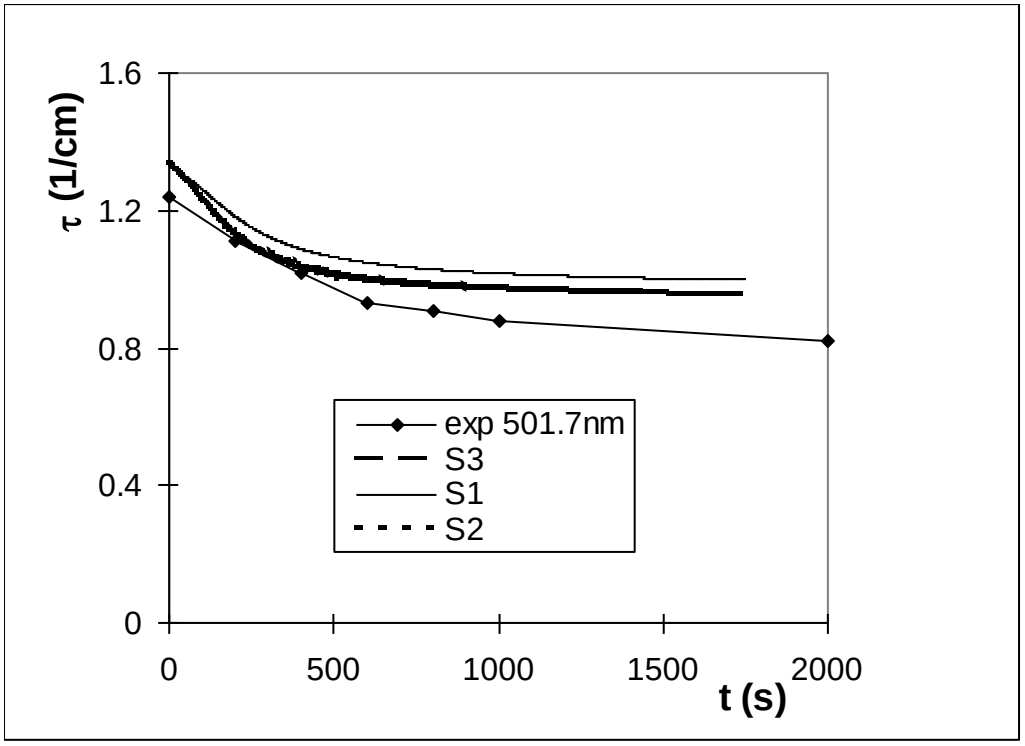
τ (1/cm)
1.6
1.2
0.8
0.4
0
0
500
1000
1500
2000
t (s)
exp 501.7nm
S3
S1
S2

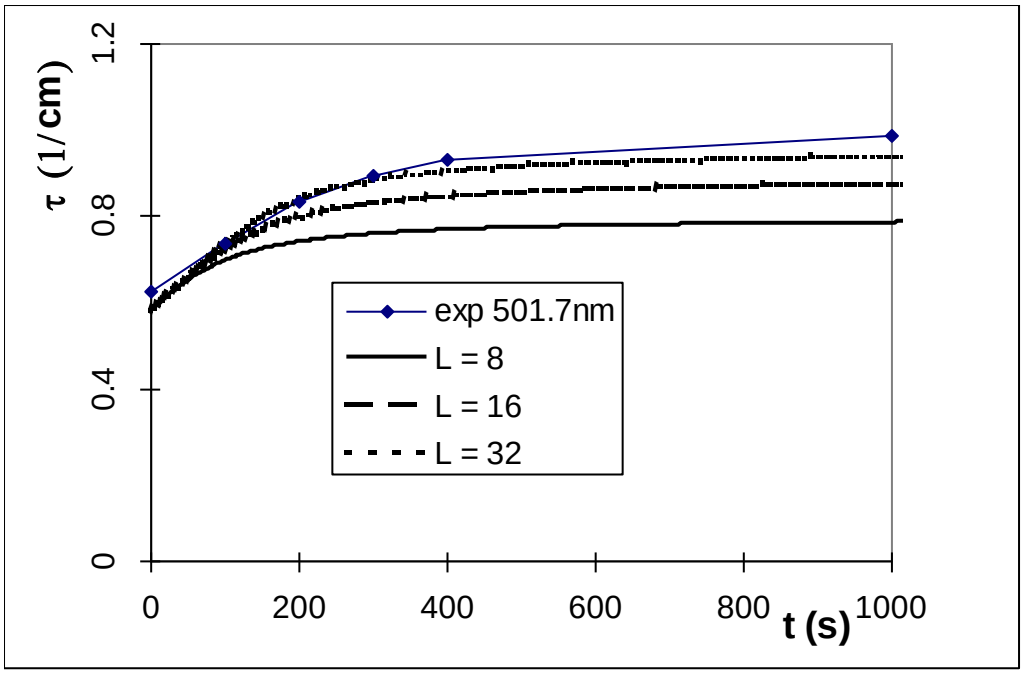
τ (1/cm)
1.2
0.8
0.4
0
0
200
400
600
800
1000
t (s)
exp 501.7nm
L = 8
L = 16
L = 32

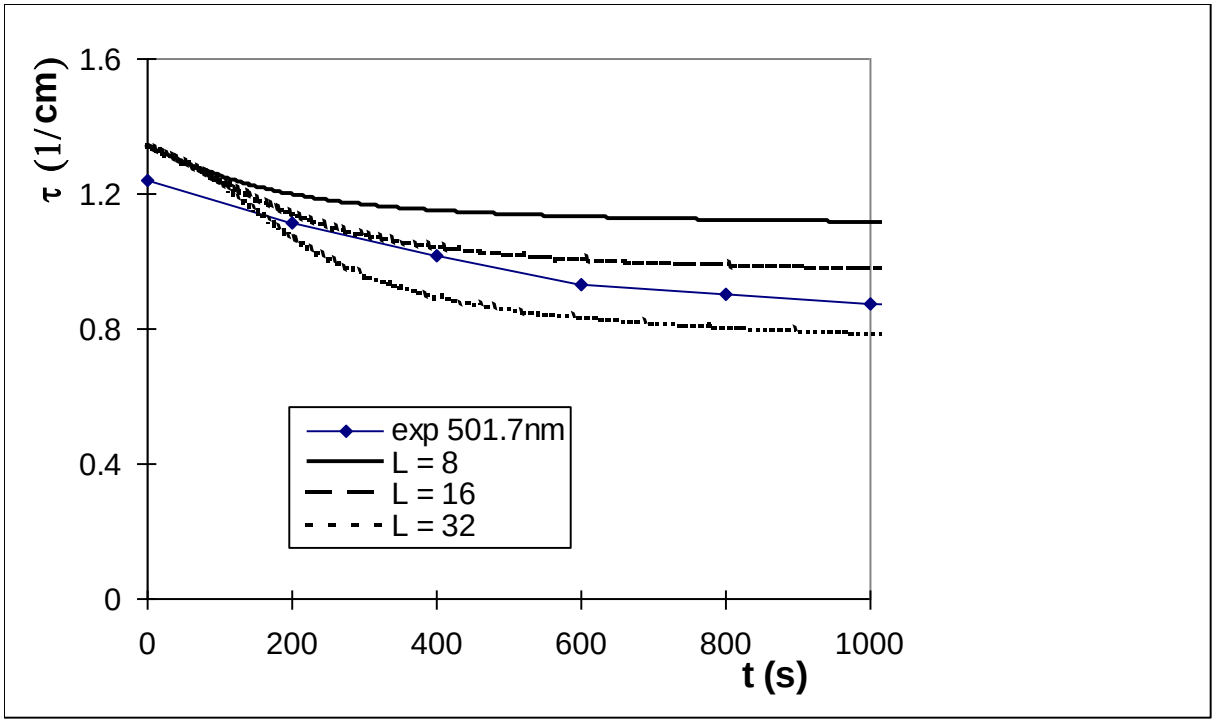
τ (1/cm)
1.6
1.2
0.8
0.4
0
0
200
400
600
800
1000
t (s)
exp 501.7nm
L = 8
L = 16
L = 32

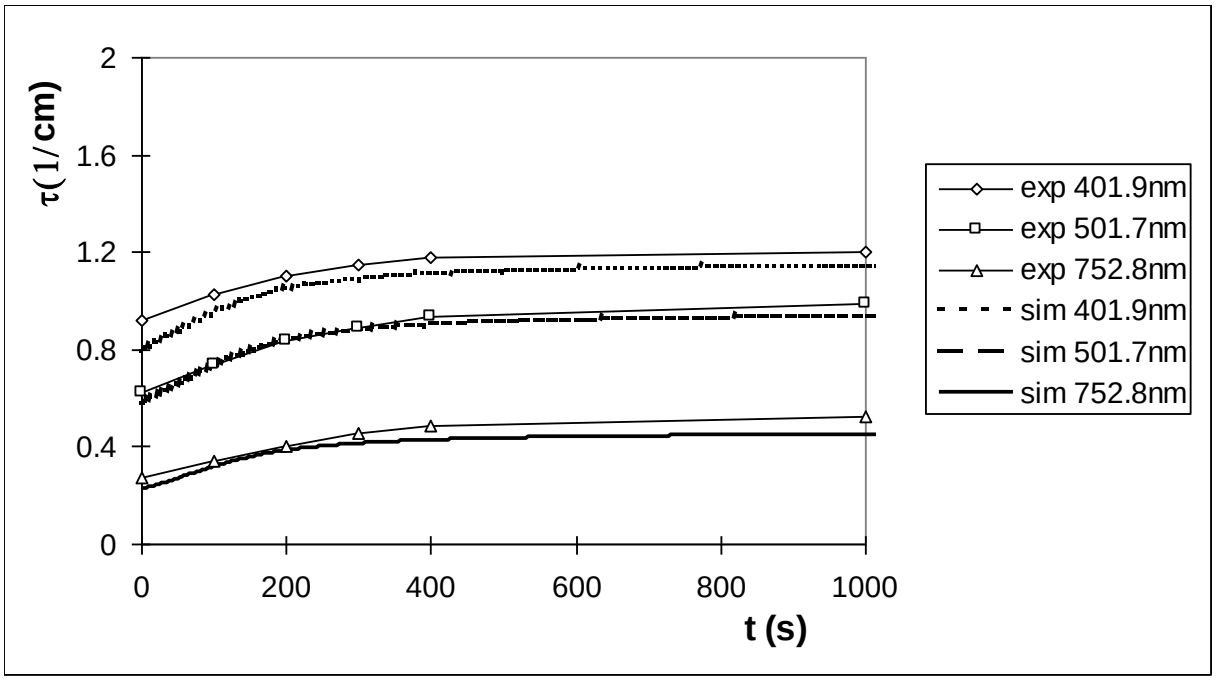
τ(1/cm)
2
1.6
1.2
0.8
0.4
0
0
200
400
600
800
1000
t (s)
exp 401.9nm
exp 501.7nm
exp 752.8nm
sim 401.9nm
sim 501.7nm
sim 752.8nm

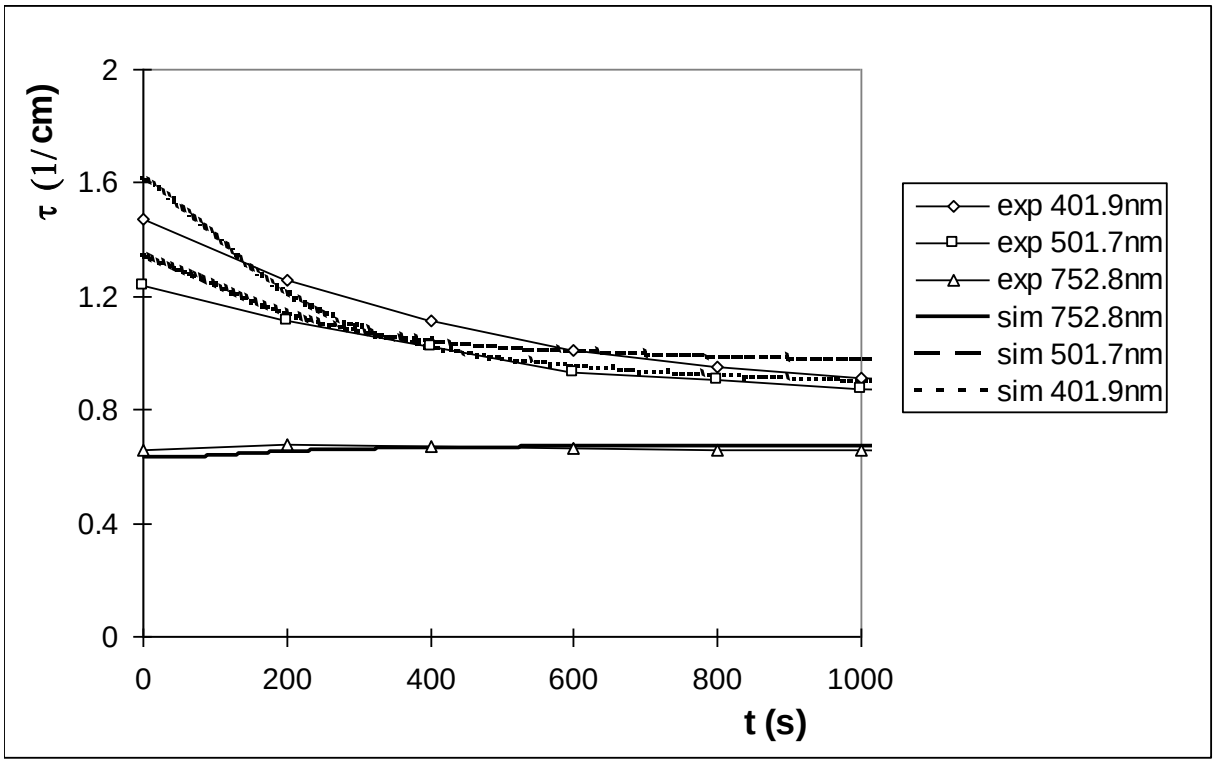
τ (1/cm)
2
1.6
1.2
0.8
0.4
0
0
200
400
600
800
1000
t (s)
exp 401.9nm
exp 501.7nm
exp 752.8nm
sim 752.8nm
sim 501.7nm
sim 401.9nm

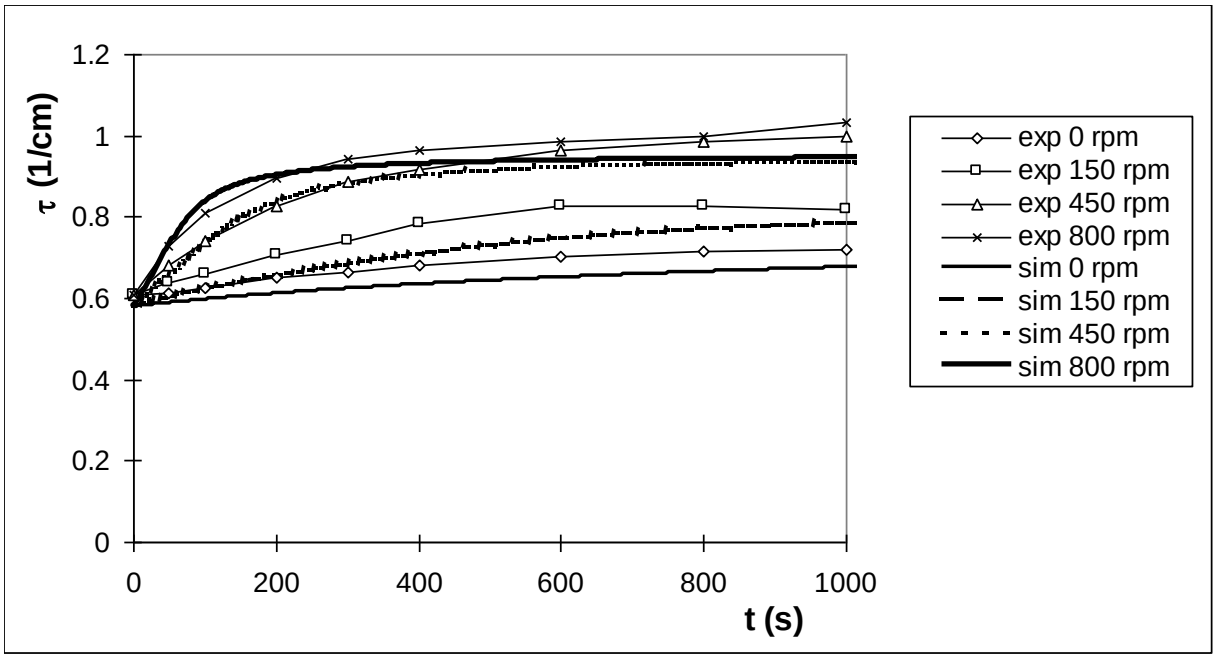
1.2
1
0.8
0.6
0.4
0.2
0
τ (1/cm)
0
200
400
600
800
1000
t (s)
exp 0 rpm
exp 150 rpm
exp 450 rpm
exp 800 rpm
sim 0 rpm
sim 150 rpm
sim 450 rpm
sim 800 rpm